Fluorescence lifetime imaging unravels the pathway of glioma cell death upon hypericin-induced photodynamic therapy

Miriam C. Bassler[1,2], Jonas Hiller[2*], Frank Wackenhut[1**], Sven zur Oven-Krockhaus[2], Philipp Frech[2], Felix Schmidt[2], Christoph Kertzscher[2], Tim Rammler[2], Rainer Ritz[3], Kai Braun[2], Marcus Scheele[2], Alfred J. Meixner[2**], Marc Brecht[1,2**]*

[1]*Process Analysis and Technology (PA&T), Reutlingen University, Alteburgstr. 150, 72762 Reutlingen, Germany*

[2]*Institute of Physical and Theoretical Chemistry, University of Tübingen, Auf der Morgenstelle 18, 72076 Tübingen, Germany*

[3]*Department of Neurosurgery, Schwarzwald-Baar Clinic, 78052 Villingen-Schwenningen, Germany*

---

*These authors contributed equally to this work.

**Corresponding authors

Keywords: hypericin, fluorescence lifetime imaging microscopy, photodynamic therapy

Supplementary information

Section 1 – Fundamentals of Fluorescence Lifetime Data Acquisition and Analysis

The following section aims to provide the basics of time-correlated single photon counting (TCSPC) data acquisition, analysis, and interpretation. However, given that time-resolved photoluminescence has been an active area of research for over 40 years, the discussion presented here is not exhaustive. For a general overview of molecular fluorescence spectroscopy, we recommend the textbook by J. R. Lakowicz.[1] Textbooks specializing on TCSPC are found in ref. [2, 3].

Section 1.1 – The Fluorescence Lifetime

Following a hypothetical, d-pulse excitation of an ensemble of a fluorophore at $t = 0$, the excited states of the individual quantum systems relax to the ground state through radiative and non-radiative pathways. The term radiative relaxation refers to deactivation processes by fluorescence or phosphorescence. The collective term non-radiative relaxation is employed to describe all remaining pathways that depopulate an excited state without light emission.

The lifetime of an excited electronic state can be understood as the average time the quantum system remains in that excited state before relaxing to the ground-state. The non-definiteness of this time interval is fundamentally due to the quantum nature of the system and is not only observed for ensembles but also when repeatedly probing the excited state kinetics of a single fluorophore.

If the measurable temporal evolution of the photoluminescence intensity *I(t)* emitted by a quantum system is directly proportional to the systems excited state population, we can describe any photoluminescence (PL) intensity decay as:

$$I(t) = A \sum_{n=1}^{m} a_n \, e^{-t/\tau_n}$$

$$with: \sum_{n=1}^{m} a_n = A = I(0) = 1,$$

where n are the individual excited states contributing to the overall (m-exponential) PL intensity decay with the photoluminescence lifetime τ_n. The photoluminescence lifetime is to be understood as the average time the quantum system remains in a particular excited state prior to ground-state relaxation via the emission of a photon. The terms a_n denote amplitude weighting fractions, the sum of which must be equal to the total amplitude A. For convenience, the total amplitude is typically normalized to 1.

The photoluminescence lifetime of an excited state, which is the average time the quantum system remains in that excited state prior to ground-state relaxation by way of PL emission, can be expressed as follows:

$$\tau_n = \frac{1}{k_{r,n} + k_{nr,n}}$$

Under the chosen experimental conditions, the organic dyes used in this study (hypericin, propidium iodide, resorufin) adhere to Kasha's rule, that in its original formulation, states that "the emitting electronic level of a given multiplicity is the lowest excited level of that multiplicity".[4] Consequently, the individual dyes display monoexponential PL decays, with the emission originating from their respective singlet one (S1) states. Consequently, the photoluminescence decay of a mixture of these dyes displays an exponentiality equal to the number of dyes contributing to the recorded PL.

Depending on how the contributions of the individual lifetimes are weighted, one can compute different average lifetimes for a multiexponential decay. Most commonly, the intensity weighted average lifetime τ_{AvInt} and the amplitude weighted average lifetime τ_{AvAmp} are used. They are calculated according to the following equations:

$$\tau_{AvInt} = \frac{\int_0^{\infty} t \sum_{n=1}^{m} a_n e^{-t/\tau_n} dt}{\int_0^{\infty} \sum_{n=1}^{m} a_n e^{-t/\tau_n} dt} = \frac{\sum_{n=1}^{m} a_n \tau_n^2}{\sum_{n=1}^{m} a_n \tau_n}$$

$$\tau_{AvAmp} = \frac{\sum_{n=1}^{m} a_n \tau_n}{\sum_{n=1}^{m} a_n = 1} = \sum_{n=1}^{m} a_n \tau_n$$

Weighing the individual summands according to their respective amplitude fractions, as it is done in calculating τ_{AvAmp} is intuitive. To understand the intensity weighing in calculating τ_{AvInt}, consider the biexponential PL decay shown in Figure S1.1.

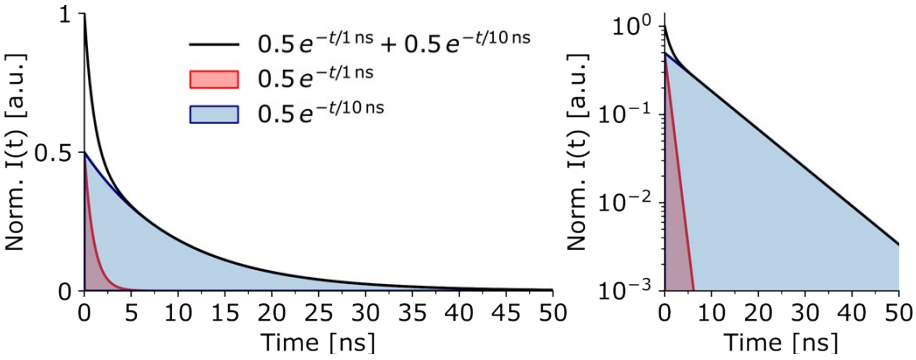

Figure S1.1: *Individual contributions to a simulated biexponential PL decay of two summands consisting of equal amplitude fractions and the lifetimes* τ_1 *= 1 ns and* τ_2 *= 10 ns, respectively. The decays are plotted on a linear (left) and semi-logarithmic (right) scale.*

While the amplitude fractions determining the initial decay contribution of the summands are equal, the contribution of the summand containing the shorter lifetime (depicted in red) vanishes fast, resulting in the summand containing the longer lifetime (depicted in blue) to be the major contribution to the overall PL decay. To account for that, in calculating the intensity weighted average lifetime, each lifetime is weighted by its relative contribution to the total decay. As a result, when calculating τ_{AvInt}, summands containing long lifetimes are weighted more heavily than those containing shorter lifetimes.

There is no generally preferred average lifetime and the non-trivial question which to use as input for calculations requiring an average lifetime value depends on the information that one wants to extract from the decay curve. This is shown for various examples in an article by A. Sillen and Y. Engelborghs.[5] In this manuscript, the intensity weighted average lifetime was chosen as the color contrast in lifetime imaging microscopy.

Section 1.2 – Measuring the Photoluminescence Lifetime using Time-Correlated Single Photon Counting

The fluorescence lifetime data presented in this manuscript was recorded by time-correlated single photon counting (TCSPC), the most commonly employed time-domain method for recording temporally resolved photoluminescence.

The acquisition principle of a TCSPC measurement is schematically illustrated in Figure S1.2. A pulsed light source (typically a laser) is used to excite a suitable luminescent sample, and subsequently emitted photons are recorded by a single photon detector. The pulsed laser and the detector are connected by TCSPC electronics, functioning as an extremely accurate timekeeping device. The temporal difference between a precisely timed laser pulse emission event and luminescence photon detection event is recorded and assigned to a histogram bin of predefined width. By virtue of the periodicity of the pulsed laser emission, such data can be collected for a great number of excitation-detection cycles and a so called TCSPC histogram containing the photoluminescence decay of the sample is recorded.

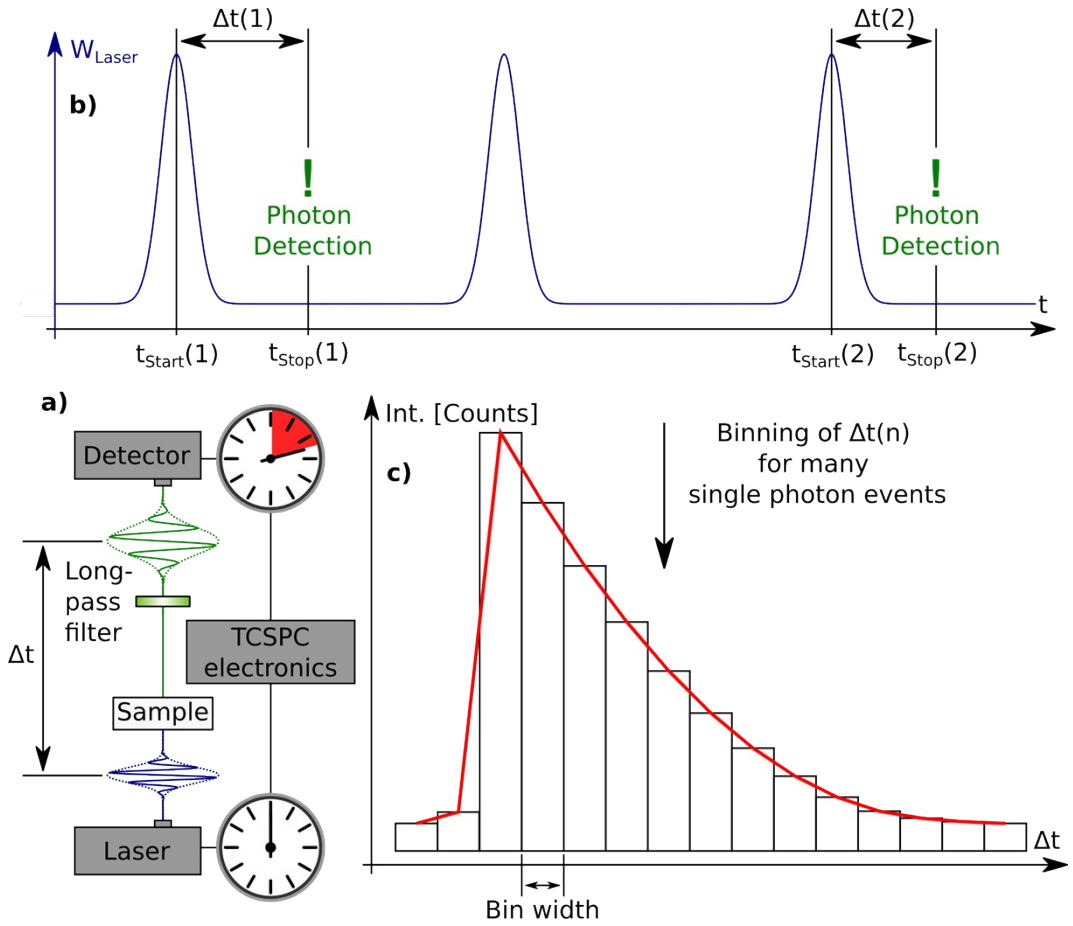

Figure S1.2: *The acquisition principle of TCSPC data. A) Hardware involved in a TCSPC experiment. B) Repetitive timing of single photon arrival times at a detector in reference to the excitation laser pulse. C) Shape of a TCSPC histogram, where the channel or bin width is drastically exaggerated for illustrative purposes.*

Section 1.3 – Analysis of TCSPC Data

The recorded decay intensity $D(t)$ is a convolution of the photoluminescence decay $f(t)$ and the instrument response function $IRF(t)$.

$$D(t) = f(t) * IRF(t)$$

The convolution of two functions is defined by the convolution integral:

$$f(t) * g(t) = \int_0^t f(u)\, g(t-u)\, du\,,$$

where u is a dummy variable of integration. The IRF is a convolution of the temporal profiles of all components employed in the TCSPC data acquisition. Typically, the most significant contributions to the IRF arise from the temporal profile of the pulsed excitation laser, the timing accuracy of the employed single photon detector and the rise/fall-time of the electric signals of the TCSPC electronics.

To evoke a graphical intuition for this operation, the convolution of an exponentially decaying function with a narrow Gaussian, which is used to approximate the profile of an IRF, is displayed in Figure S1.3.

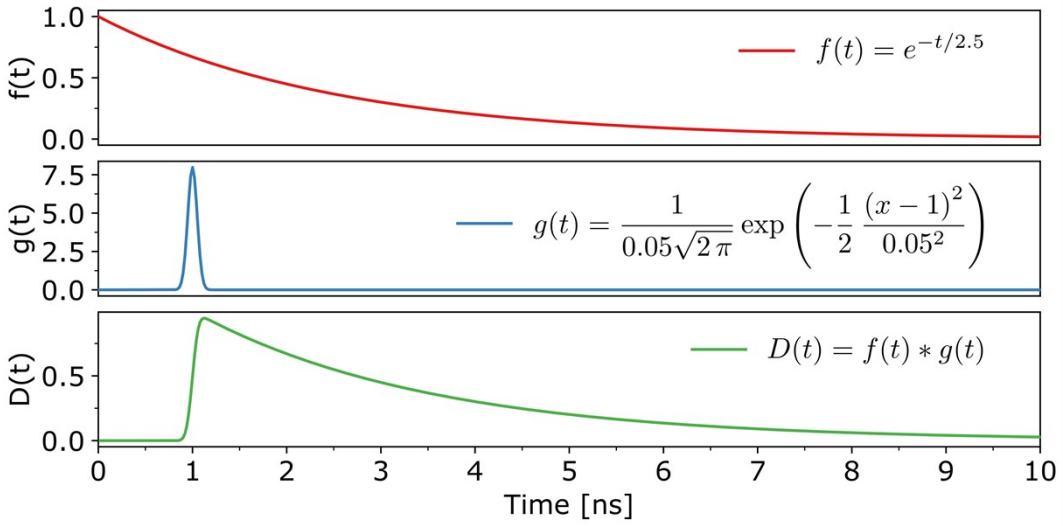

Figure S1.3: *Exemplary convolution of an exponential decay function with a narrow Gaussian, which serves as an approximate representation of an IRF. The resulting convoluted function approximates the shape of an experimental TCSPC histogram without background and noise.*

TCSPC data analysis is typically done by performing a calculation that allows one to factor out the influence of the IRF on an experimental histogram and therefore obtain the true PL decay of a sample or by directly fitting the exponentially decaying part of the TCSPC histogram (tailfitting).

The inverse operation of a convolution is appropriately named a deconvolution. In principle, several direct deconvolution techniques can be used to extract the individual contributions to a convoluted function. However, the data in an experimental TCSPC histogram, which is obtained through a finite number of discrete measurements is neither complete nor free from noise. For this reason, while feasible, direct deconvolution methods are mathematically challenging.[6, 7]

In this work, the TCSPC data of the individual dyes was analyzed using the most commonly employed iterative reconvolution method as it is implemented in the SymPhoTime64 (Picoquant) software package. Importantly, the terms deconvolution and reconvolution are not synonyms and should not be confused. Iterative reconvolution works by assuming a model exponential decay function with predefined exponentiality, convoluting this model function with an experimentally acquired IRF, and then iteratively improving the parameters a_n and τ_n of the assumed decay function to fit the measured data by a statistical fitting procedure. IRFs were recorded by detecting the excitation laser scattering from a glass coverslip.

Evaluating the goodness of fit is not trivial and a variety of methods can be employed to do so. In this work, the goodness of fit is evaluated by the so-called reduced chi-squared, denoted as χ_r^2, which is the optimization parameter for least squares fitting adjusted for Poisson statistics. χ_r^2 is calculated by the SymPhoTime64 (Picoquant) software package as follows:

$$\chi_r^2 = \frac{1}{N-p}\sum_i R(i)^2$$

$$with: R(i) = \frac{Decay(i) - Fit(i)}{\sqrt{Decay(i)}},$$

where N is the number of fitted channels (bins in the TCSPC histogram), p is the number of fitted parameters, $R(i)$ is the weighted residual for the i-th channel, $Decay(i)$ is the intensity measured for the i-th channel and $Fit(i)$ is the intensity of the fit for the i-th channel.

A good fit is indicated by a value of χ_r^2 approaching 1. An additional plot of $R(i)$ vs time highlights the quality of the fit for each individual channel of the histogram and can be displayed alongside the fitted function. Observing no trend or pattern but only random fluctuations around 0 for the plot of $R(i)$ vs time is another indicator of a good fit.

Section 2 – TCSPC Histograms of the Individual Dyes and the Fits Thereof

To obtain appropriate lifetime values of the individual dyes for the purpose of fitting FLIM images containing a mixture of those dyes, the TCSPC histograms of resorufin and hypericin were acquired in cell culture medium. As propidium iodide is only strongly fluorescent when intercalating into DNA and/or RNA the TCSPC histogram depicted in Figure S2.3 was acquired by recording the PL emitted by the nucleus of a dead glioblastoma cell in PI enriched cell culture medium.

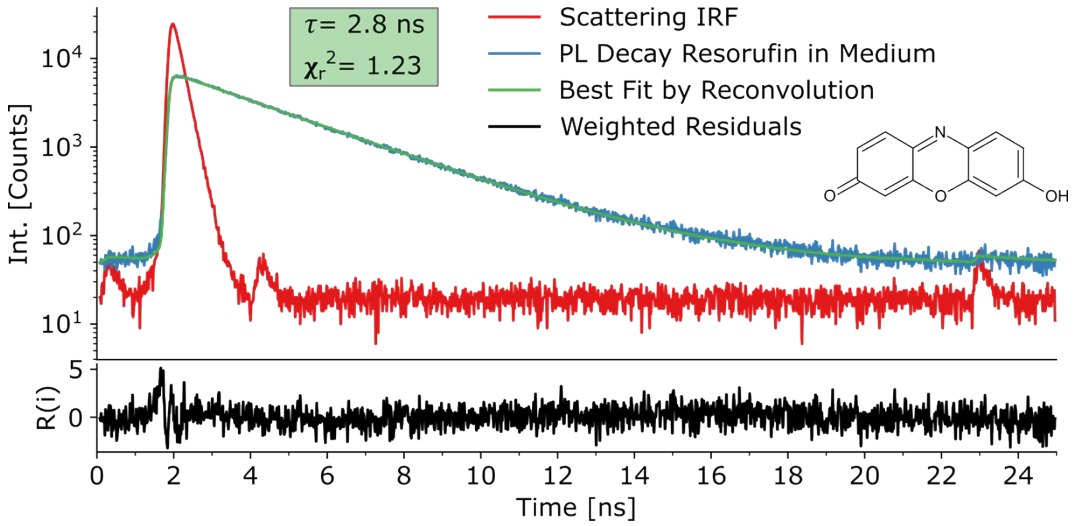

Figure S2.1: *Experimental TCSPC histogram (blue) and fit function (green) of a dilute solution of resorufin in cell culture medium. The lifetime of 2.69 ns was obtained by iterative reconvolution with an appropriately acquired IRF (red) for the choice of a biexponential decay model. Relevant acquisition parameters:* λ_{exc}*= 405 nm,* λ_{det} *= upwards of 532 nm (long pass filter), pulse rate = 40 MHz, channel width = 16 ps.*

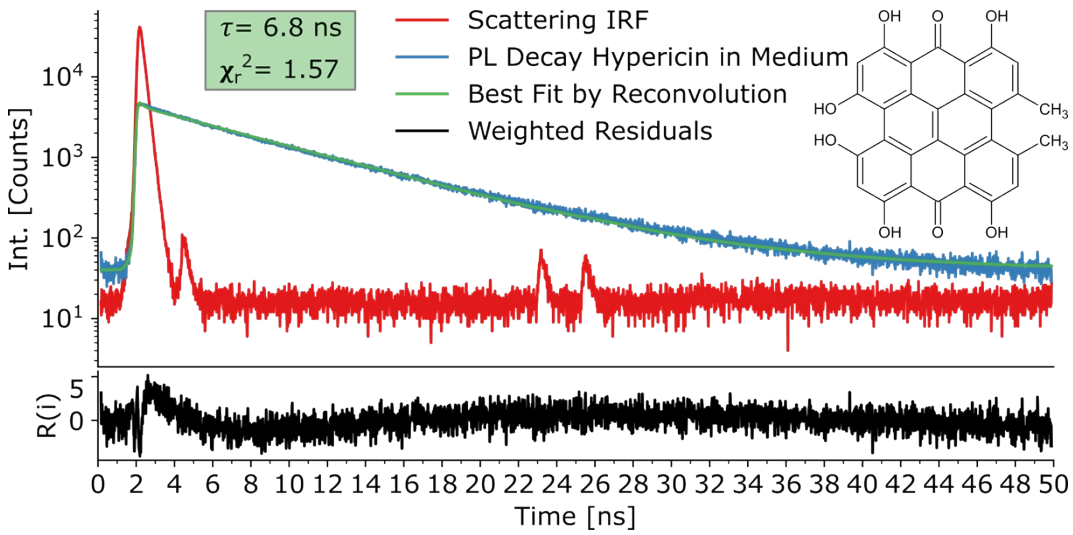

Figure S2.2: *Experimental TCSPC histogram (blue) and fit function (green) of a dilute solution of hypericin in cell culture medium. The lifetime of 6.58 ns was obtained by iterative reconvolution with an appropriately acquired IRF (red) for the choice of a biexponential decay model. Relevant acquisition parameters:* λ_{exc}*= 405 nm,* λ_{det} *= upwards of 532 nm (long pass filter), pulse rate = 20 MHz, channel width = 16 ps.*

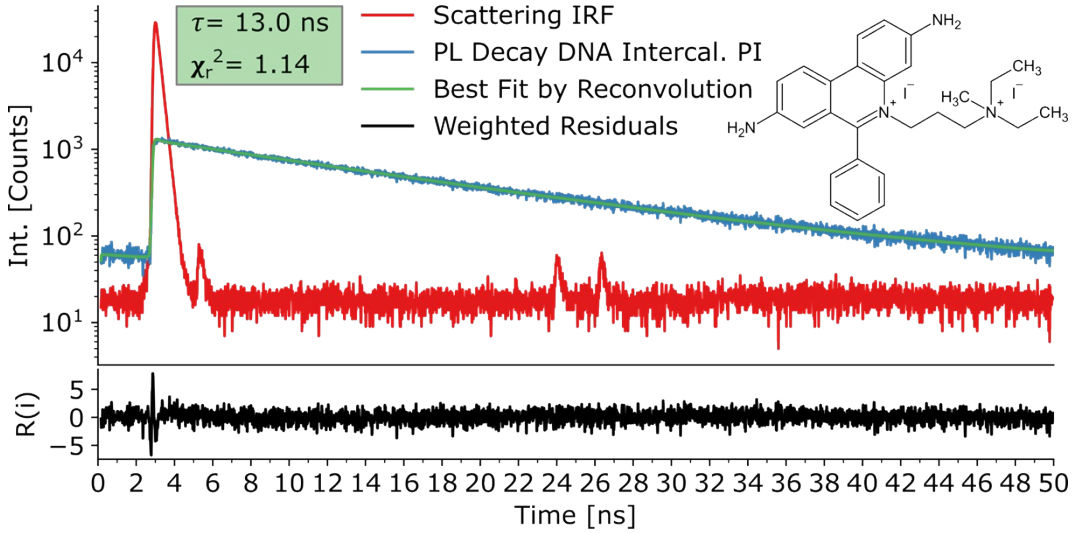

Figure S2.3: *Fit resulting from iterative reconvolution of an experimental TCSPC histogram of propidium iodide intercalated into a cell nucleus with an appropriately acquired IRF for the choice of a biexponential decay model. Relevant acquisition parameters:* λ_{exc}*= 405 nm,* λ_{det} *= upwards of 532 nm (long pass filter), pulse rate = 20 MHz, channel width = 16 ps.*

It should be noted that a second exponent was supplied in the iterative reconvolution process of all dyes to accurately fit the time channels containing the very onset of the TCSPC histograms and therefore obtain a high-quality fit of the underlying PL decay. This often observed “non-physical” exponent is caused by inaccuracies in recording the IRF (the temporal profile of the single photon avalanche diode is dispersive). For all three dyes, the fitted lifetime of this “non-physical” exponent is far below the resolution of the employed instruments (approx. 5 ps) and can be neglected. The exact same τ values for the dyes are obtained by tailiftting the PL decays using a monoexponential decay model. This is to be expected as in our instrument the IRF only influences the onset and a few early channels of the PL decay. The PL lifetime of a dye depends on the dye’s immediate dielectric environment. Figure S2.4

shows the PL decay of Hypericin in DMSO and the fit thereof. The fluorescence lifetime of hypericin in DMSO is considerably shorter than in cell culture medium.

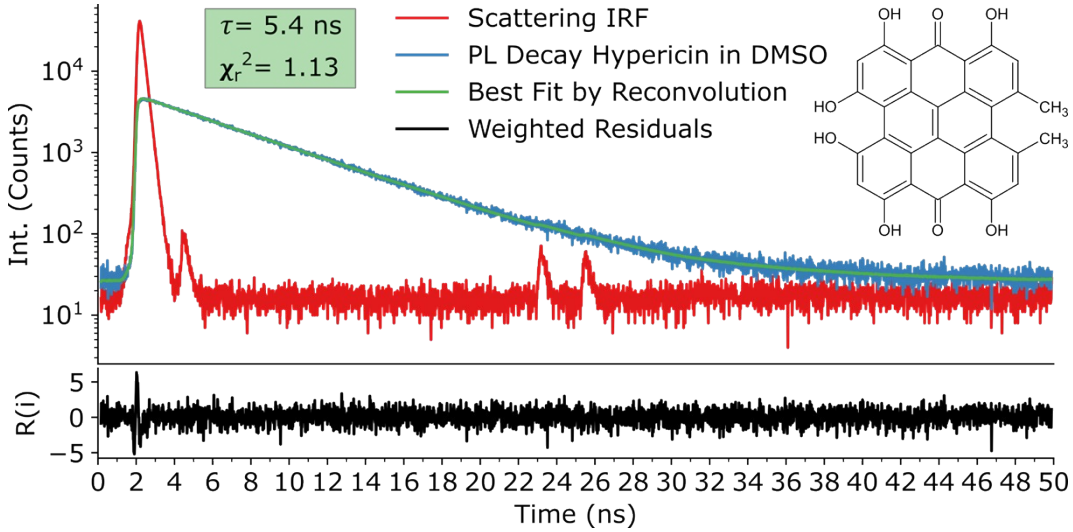

Figure S2.4: *Fit resulting from iterative reconvolution of an experimental TCSPC histogram of of a dilute solution of hypericin in DMSO. The lifetime of 5.4 ns was obtained by iterative reconvolution with an appropriately acquired IRF (red) for the choice of a biexponential decay model. Relevant acquisition parameters:* λ_{exc}*= 405 nm,* λ_{det} *= upwards of 532 nm (long pass filter), pulse rate = 20 MHz, channel width = 16 ps.*

Section 3 – Fluorescence Lifetime Imaging Microscopy

Fluorescence lifetime imaging microscopy (FLIM) data is recorded by scanning the sample within an area of interest over the diffraction limited focal spot and recording a TCSPC histogram at each pixel. The area of interest (upper limit is given by the scanning range of the employed piezo nano-positioning stages), pixel size and dwell time (acquisition time) per pixel are specified prior to the acquisition. The pixel size of the images presented in this work was chosen according to the Nyquist criterion (e.g., 300x300 pixels for a 24x24 µm image). A schematic of the FLIM data acquisition process is shown in Fig. S3.1. The actual FLIM images are then generated by plotting a chosen type of photoluminescence lifetime data, extracted from the individual histograms at each pixel as the contrast value of the respective pixel.

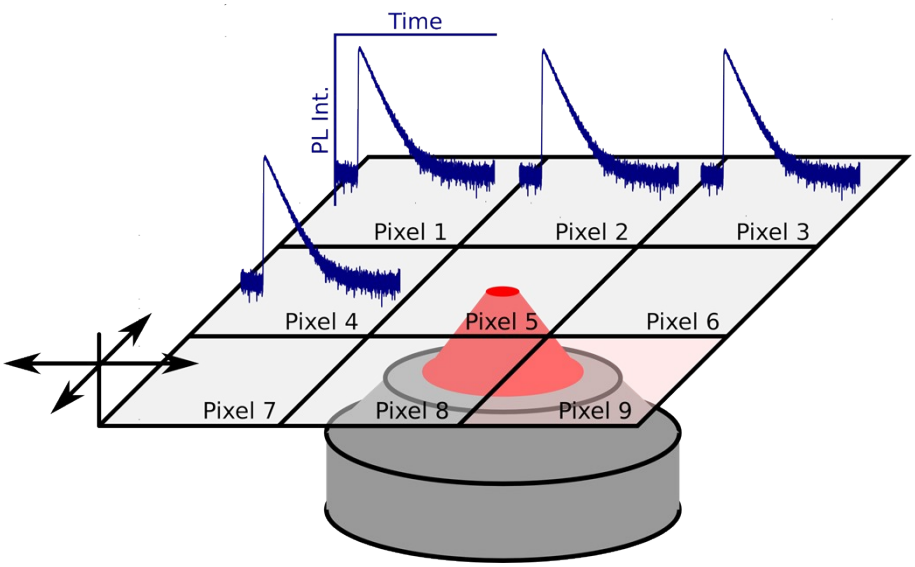

Figure S3.1: *Schematic of the FLIM measurement principle. The desired scan range is subdivided into a grid consisting of a specified number of pixels (3x3 pixels in this case). The nano-positioning stage is used to move each pixel into the diffraction limited focal spot, where a TCSPC histogram is accumulated for a prespecified amount of time. After this so-called dwell time the sample scanning continues until TCSPC histograms for all pixels are acquired.*

Section 3.1 – Exemplary FLIM Analysis and the Problem of Correlation Between the Fitted Parameters

The employed SymPhoTime64 (Picoquant) software package can be used to quickly calculate the so-called fast lifetime at every pixel of a FLIM image. The fast lifetime is to be understood as an estimate of the intensity weighted average lifetime obtained from a TCSPC histogram without fitting of the data using a model decay function. It is the average photon arrival time after the excitation pulse and is therefore equal to the channel width (timing resolution) multiplied by the distance between the onset of the decay curve and the barycenter of the TCSPC histogram (the channel associated with the average number of photon counts).

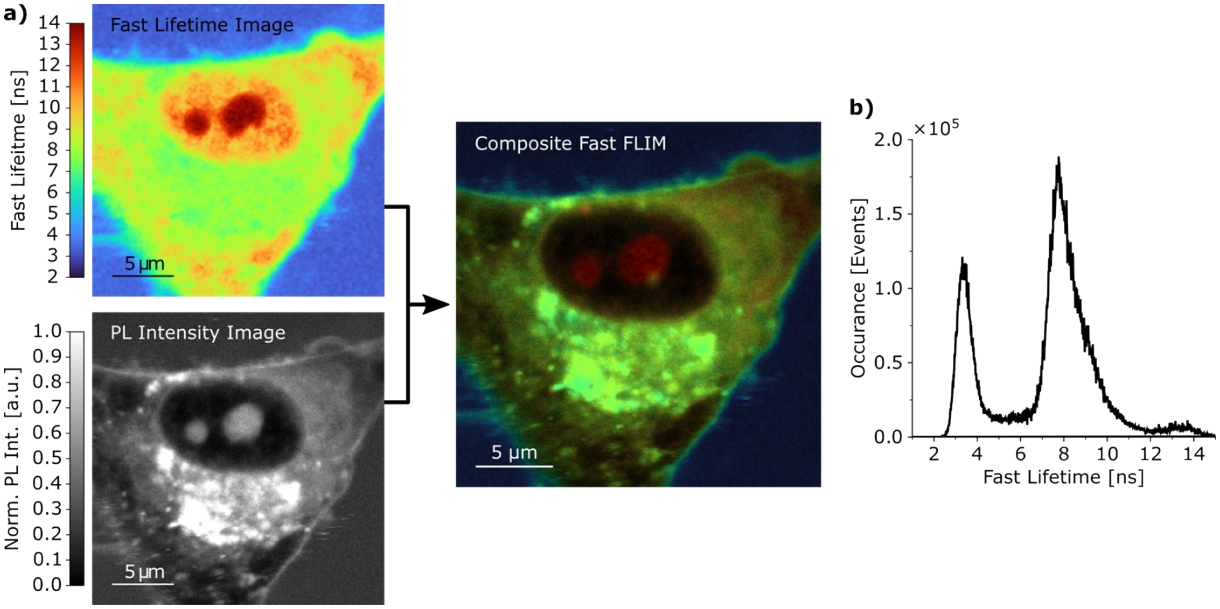

Figure S3.2: *a) The recorded PL Intensity and fast lifetimes extracted from the TCSPC histograms at each pixel can be combined to form a composite image, where the contrast is given by the pixel's associated fast lifetime value and the brightness is determined by the pixel's fluorescence intensity. b) An occurrence plot that displays how many photons with the associated fast lifetime (arrival time after the excitation pulse) are recorded in the image.*

While this analysis is fast and gives a good qualitative impression of the samples PL decay, no information beyond an estimate of the average lifetime can be extracted. To obtain more accurate lifetime values and further information such as the relative contributions of the individual dyes, the FLIM images presented in this work were subjected to a pixel-by-pixel fit.

When analyzing these FLIM images via pixel-by-pixel fitting, however, we are faced with a problem. The emission of a mixture of the employed dyes is recorded in the individual noisy histograms associated with each pixel of a FLIM image of the investigated cells. The fitting parameters in the parameter estimation process of a multiexponential model decay function, namely the amplitude fractions and the photoluminescence lifetimes, are highly correlated. As a result, the effect on the overall decay curve resulting from changes in one of the fitted parameters may almost be completely compensated by simultaneous changes in the other parameters. The reader interested in this topic is referred to an article by A. Grinvald and I. Z. Steinberg[8], where this problem is nicely illustrated.

To reduce the amount of fitted parameters, the lifetime values of the individual dyes (determined by iterative reconvolution, see Figures S2.1-S2.3) were not fitted but supplied to the model decay function, while allowing for deviations of ± 0.2 ns to account for changes in the dielectric environments within the cell. As a result, only the amplitude fractions of the components are fitted, significantly decreasing the parameter correlation in the fitting process. An example of a pixel-by-pixel fitting process is displayed in Fig. S3.3.

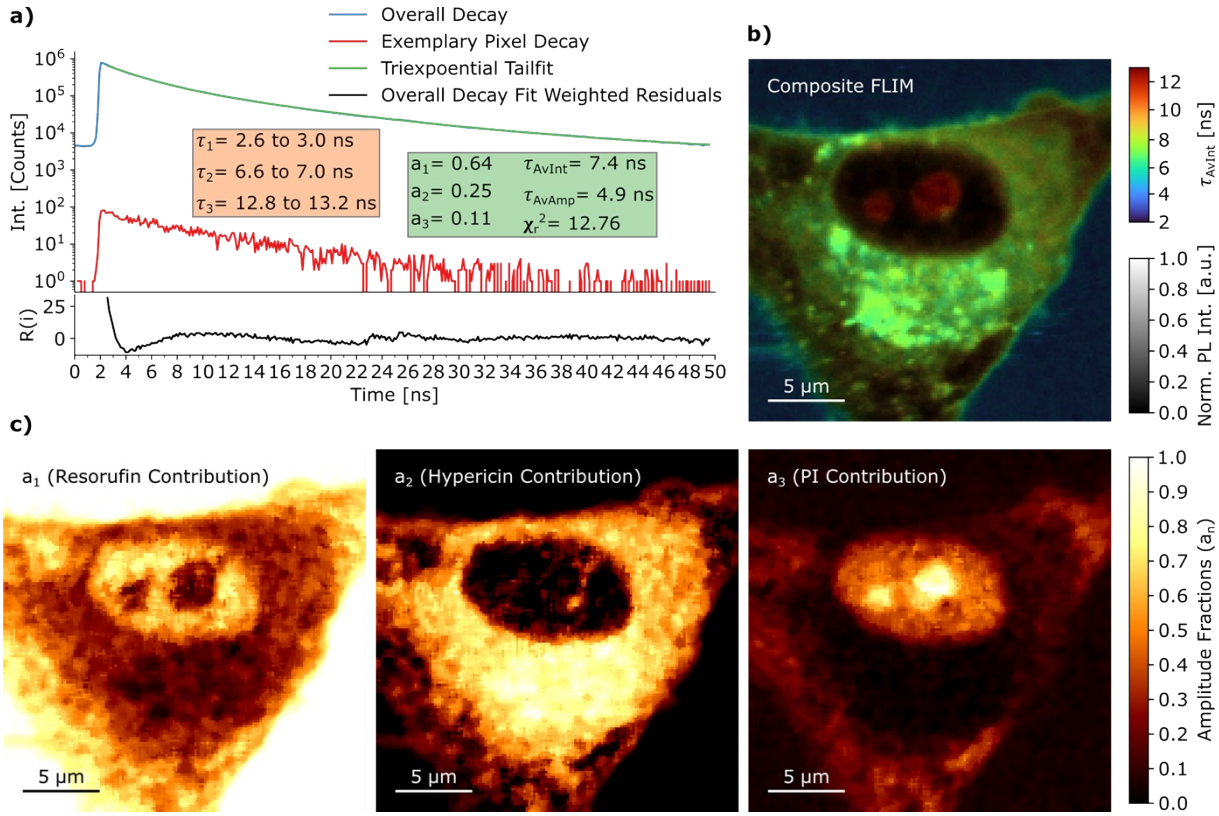

Figure S3.3: *Exemplary pixel-by-pixel fitting of an experimentally acquired FLIM image, comprised of 300x300 pixels, recorded with a channel width of 16 ps and a dwell time of 20 ms. a) TCSPC histogram and triexponential tailfit of the overall PL decay recorded in the image. The lifetime value ranges in the orange box were supplied to the model decay function, the parameters in the green box are obtained from the fit. The TCSPC histogram of an exemplary pixel after spatial and time channel binning of the pixels is displayed to give an impression of the signal-to-noise ratio of the TCSPC histograms in the pixel-by-pixel fit. b) This composite image is now a true FLIM image, where the color is given by the intensity weighted average lifetime obtained by fitting the triexponential model decay function to the PL decays of all pixels. c) The pixel-by-pixel fit returns, among other things, the amplitude fractions at each pixel. This can be used to image the contribution of the individual dyes.*

The overall decay is the sum of the decays associated with each of the 90000 pixels employed in the image acquisition. By fitting the overall decay, one obtains information about PL properties of the overall image, such as the absolute value of the fluorescence intensity emitted by each individual dye within the image. By fitting the decays contained within the individual pixels of the image pixel-by-pixel, one obtains spatially resolved information about PL originating from the sample from within that specific pixel. The FLT values represented as color contrast in the FLIM images in this work were all obtained by pixel-by-pixel fits.

A good fit of the overall decay is an indication for the supplied lifetime values of the individual dyes to be applicable to the cellular system. Accumulating a TCSPC histogram to a high signal-to-noise ratio while not acquiring with too high of a count rate (to avoid pile-up) is time intensive. As the PDT is induced while scanning the sample over the excitation laser, relatively short dwell times (of approx. 20 ms) at

each pixel are required to capture the progressing cell death over the course of multiple images. Therefore, to obtain signal-to-noise ratios of the TCSPC histograms at each pixel, adequate for fitting, spatial and time channel binning are performed prior to the pixel-by-pixel fitting.

In all composite FLIM images shown in this work, the color is given by the intensity weighted average lifetime obtained by pixel-by-pixel fitting the triexponential model decay function to the PL decays of all image pixels. The brightness is given by the overall PL intensity recorded within each pixel.

Section 4 – Additional Confocal Measurement of a Cell Incubated with Hypericin and Resorufin

In the following, an additional composite FLIM image series showing the effect of hypericin induced PDT on a single glioma cell incubated with resorufin and hypericin is depicted and discussed.

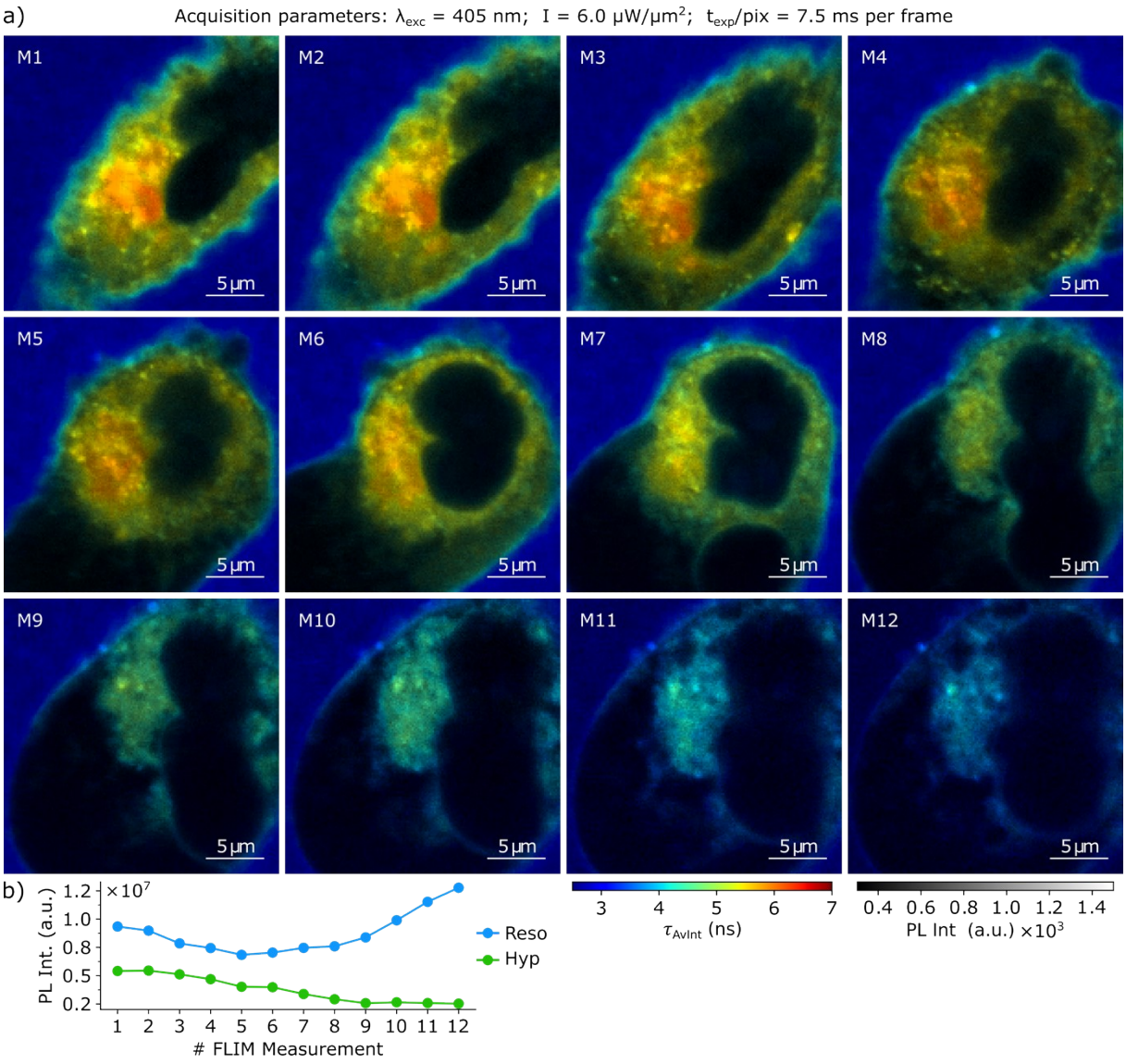

Figure S4.1: *a) Composite FLIM image series of a single glioma cell after hypericin incubation and resorufin conversion. b) The evolution of the PL intensity emitted by the individual dyes in the FLIM image series. The acquisition parameters of the imaging series are displayed above.*

The PDT induced cellular damage and death progresses similarly to the comparable measurement displayed in Fig. 2 of the main manuscript. One observes cell contraction and rounding in Fig. S4.2 a M1-M4, accompanied by the formation of small surface blebs. These blebs merge to form a large protuberance close to the ER (region of highest hypericin concentration) in M5. The swelling of the cell

progresses until the rupture of the cellular membrane around M8, which leads to flooding of the cell with surrounding medium. Here, the cell death progresses at a slower rate compared to the measurement in the main manuscript, since the overall irradiance of the cell is 23% lower. Fig. S4.2 b shows the gradual decrease of the hypericin PL intensity in the individual FLIM images. The resorufin PL intensity initially also decreases due to the expansion (protuberance) of the cell, leading to less overall resorufin being present in the scan area, and then increases from M8 onwards as a result of the flooding of the cell with surrounding medium.

Section 5 – Confocal Control Measurements of Glioma Cells Incubated without Hypericin / Control Measurements

To ensure that the reproducibly observed cell death is caused by hypericin induced PDT and not solely a result of photodamage caused by the laser irradiation, control measurements of glioma cells that were not incubated with hypericin were performed at laser powers which were larger than the 7-9 µW/µm² at λ_{exc} = 405 nm used for the induction of hypericin PDT. To ensure comparability between these control measurements and the measurements of cells containing the photosensitizer hypericin, the remaining acquisition parameters were not changed.

Figure S5.1 displays a composite FLIM image series of a single glioma cell incubated with only PI. Only very little PI is found in the cell as indicated by the low overall PL intensity. Under these low fluorescence conditions, the contribution of the cells autofluorescence to the overall PL decay can no longer be neglected. Therefore, the pixel-by-pixel fit decays of the FLIM images presented in this section were fitted using a biexponential decay model. Within the composite FLIM images, steady state fluorescence spectra were recorded at the marked locations and are displayed in Figure S5.2.

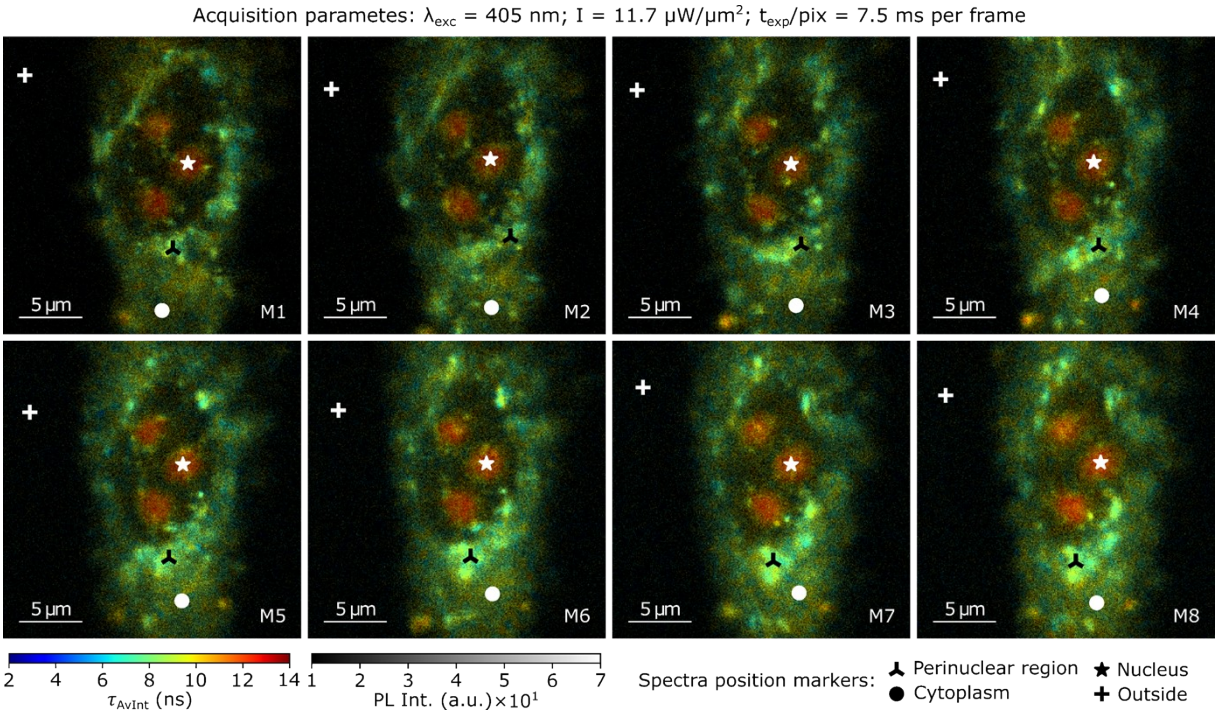

Figure S5.1: *Composite FLIM image series of a single glioma cell after PI supplementation. The spectra corresponding to the position markers are displayed in Figure S5.2.*

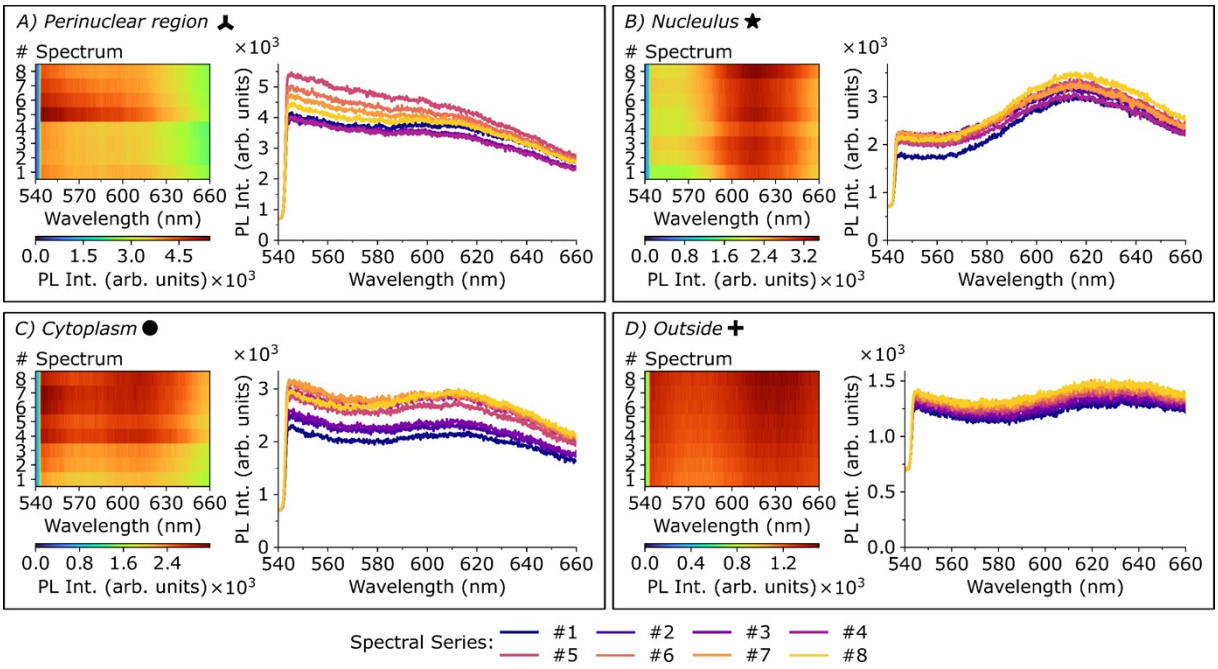

Figure S5.2: *Spatially resolved fluorescence spectra recorded on the exact locations of the corresponding markers in Figure S5.1. All spectra were acquired at the wavelength and laser power used for the FLIM image acquisition (405 nm, I = 11.7 µw/µm²) with an integration time of five second. This is five times the acquisition time that was used to record the spatially resolved spectra within the measurements that contained hypericin to compensate for the low fluorescence.*

As evident from the measurements depicted in the previous figures, we do not observe any indications of cellular damage when the cells were not incubated with the photosensitizer hypericin. As the overall fluorescence intensity under these experimental conditions is low (roughly 1% of the fluorescence recorded when all dyes are present) any increase in the uptake of PI as a result of cellular damage would result in a drastic increase of the fluorescence intensity recorded in the FLIM images or spatially resolved spectra. Indeed, from the spatially resolved spectra it is evident that the cellular autofluorescence, which manifests as a broad signal decreasing almost linearly over the entire observed spectral range from 540 to 660 nm, dominates the overall fluorescence intensity.

This raises the question of how far we can raise the irradiance before observing indications of laser induced damage to our “control” cells within the time frame of a typical FLIM series measurement. We found indications of slowly progressing cellular stress/damage at irradiances upwards of 20 µW/µm². As a reminder, 7-9 µWµm² were used to induce PDT in cells incubated with hypericin. An exemplary FLIM series measurement of a single glioblastoma cell incubated with only PI at a high irradiance of 19.6 $\mu W/\mu m^2$ is displayed in Figure S5.3.

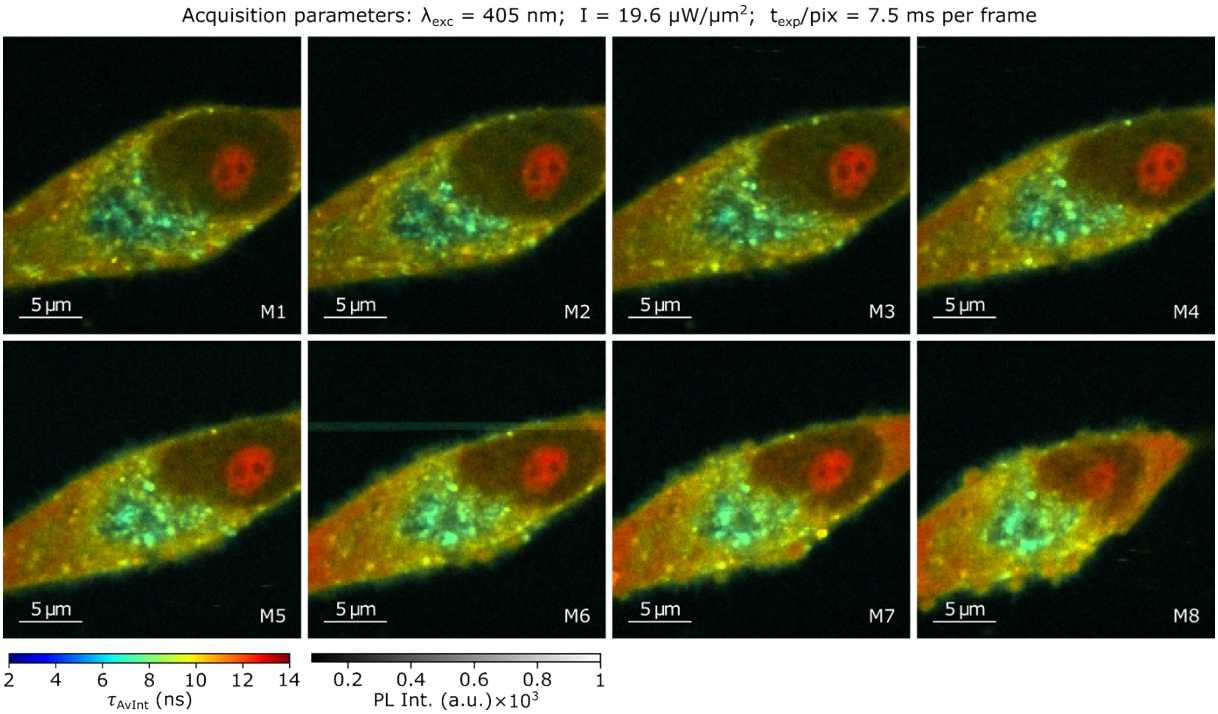

Figure S5.3: *Composite FLIM image series of a single glioma cell after PI supplementation. Due to the high irradiance, the image contrast in this series measurement is elevated compared to the FLIM series measurement in Figure S5.1.*

During the FLIM series displayed in Figure S5.3, we see a slight but gradual increase of the average fluorescence lifetime of the cell. This is caused by an increase of the concentration of PI within the cell and is therefore an indicator for cellular stress/damage. It should be noted that the laser induced photodamage observed here shows none of the characteristic morphological changes that we attribute to hypericin induced PDT and generally appears very slow and gradual. We observe no rounding, no formation of a large membrane protuberance, the ER (the region of lowest average lifetime in the individual images, adjacent to the nucleus) remains intact and the cell is not flooded with the surrounding medium.

At these high irradiance levels, we often observed control cells to evade from the scanning area and therefore the laser irradiation after some time. We did not observe such evasive attempts for cells incubated with hypericin. We speculate that hypericin induced PDT damages the glioblastoma cells in a way that drastically impedes their movement, while control cells that solely experience stress from the laser irradiation remain mobile.

We conclude that without the presence of the PDT sensitizer hypericin, we observed no significant cell damage after comparable irradiation of the single glioma cells. The morphological steps in the cell death of single glioblastoma cells discussed in this work are a direct result of hypericin induced PDT.

Section 6 - Supporting Information for Figure 3 of the Main Manuscript

The following figures supply additional information for the early, intermediate, and late stage (M1, M5, and M8) of the PDT induced cell death displayed in Fig. 3 of the main manuscript.

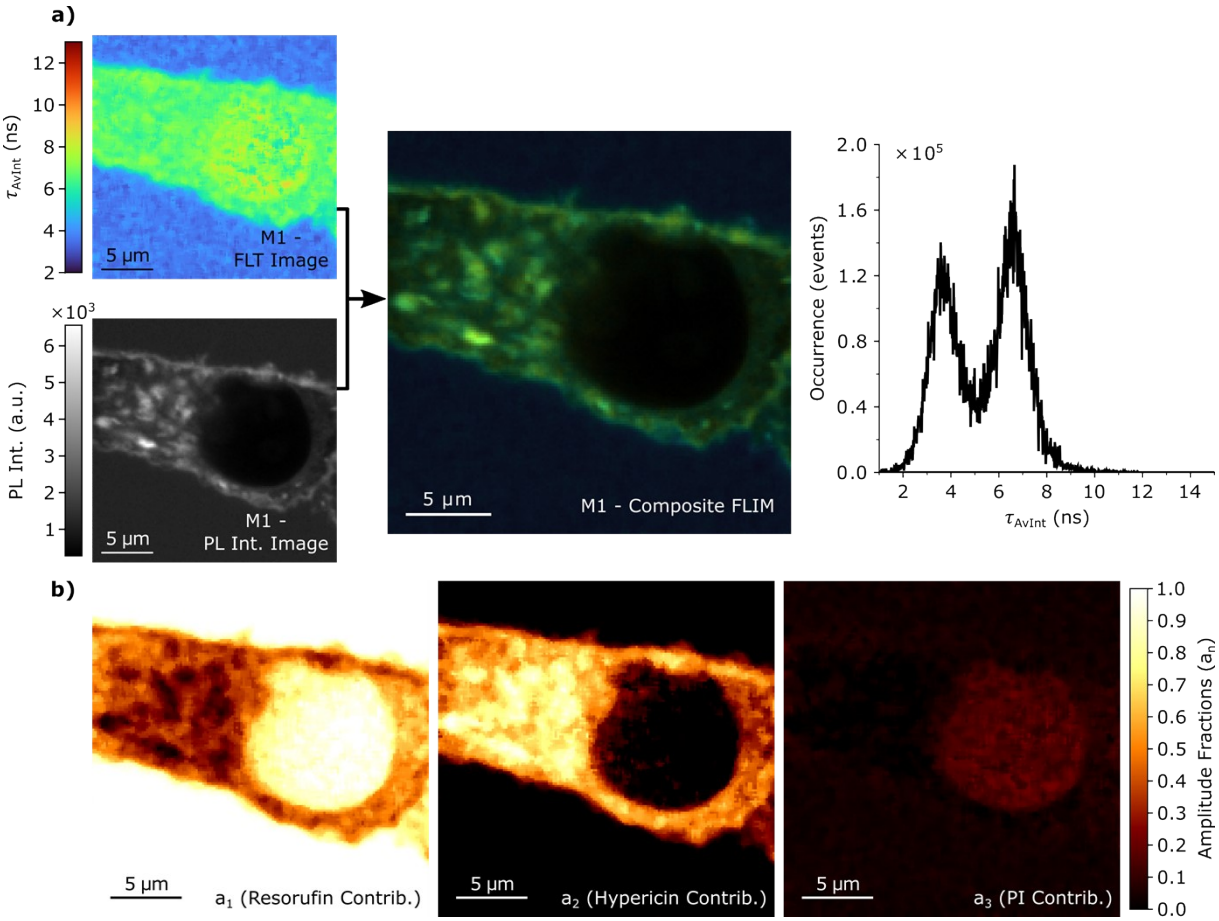

Figure S6.1: *Supplementary information for Fig. 3 (main manuscript) M1. In a) the FLT image and the PL intensity image that comprise the composite FLIM image are depicted and the occurrence plot for the image's* τ_{AvInt} *values are shown. The amplitude fraction plots in b) depict the contribution of the individual dyes to the 3-exponential fit of the overall photoluminescence decay at each pixel of the FLIM image.*

At this early stage of PDT, we can probe the location of the dyes and their respective influence on the overall PL of the (nearly) undisturbed cell. The two peaks in the occurrence plot in Fig. S6.1a at approx. 3 ns and 7 ns can clearly be assigned to resorufin and hypericin, while only a miniscule amount of PI is detected. This can also be seen in the amplitude fraction plots in Fig. S6.1b, where the fitted contribution of the individual dyes to the photoluminescence decay of each pixel are displayed. The physical relevance of the amplitude fractions is outlined in section S1.1. Resorufin mainly accumulates in the surrounding medium, while hypericin mainly accumulates in the cell's endoplasmic reticulum. However, both dyes are also found in the cell's cytoplasm. Consequently, the fluorescence lifetime of the cell's cytoplasm is a weighted average of these two lifetimes. The miniscule amount of PI already present in the undisturbed cell is located within the cell nucleus.

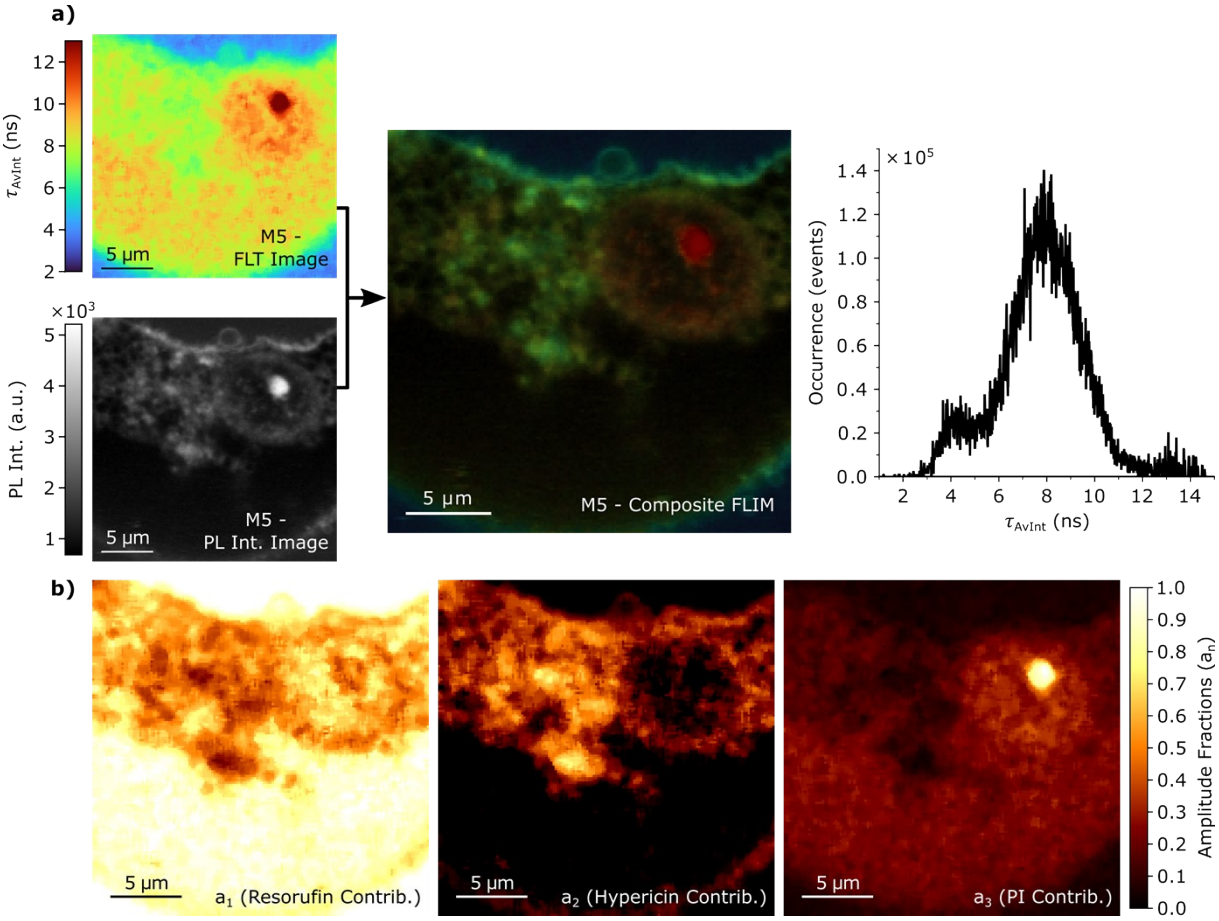

Figure S6.2: *Supplementary information for Fig. 3 (main manuscript) M5. In a) the FLT image and the PL intensity image that comprise the composite FLIM image are depicted and the occurrence plot for the image's* τ_{AvInt} *values are shown. The amplitude fraction plots in b) depict the contribution of the individual dyes to the 3-exponential fit of the overall photoluminescence decay at each pixel of the FLIM image.*

At this intermediate PDT stage, the damaging effect of PDT on the cell is clearly visible. In the occurrence plot in Fig. S6.2a the broad distribution of average lifetime values between approx. 6 and 10 ns indicates mixing of the dyes within the cell. This in conjunction with the decreasing hypericin fluorescence in the spatially resolved spectra acquired within the ER (see Fig. 4A of the main manuscript) and the smearing of the ER region in the FLIM images is a clear indicator for the disintegration of the ER. The fluorescence of PI, which now contributes to the PL of nearly the entire cell (minus the non-polar remains of the ER region), has drastically increased.

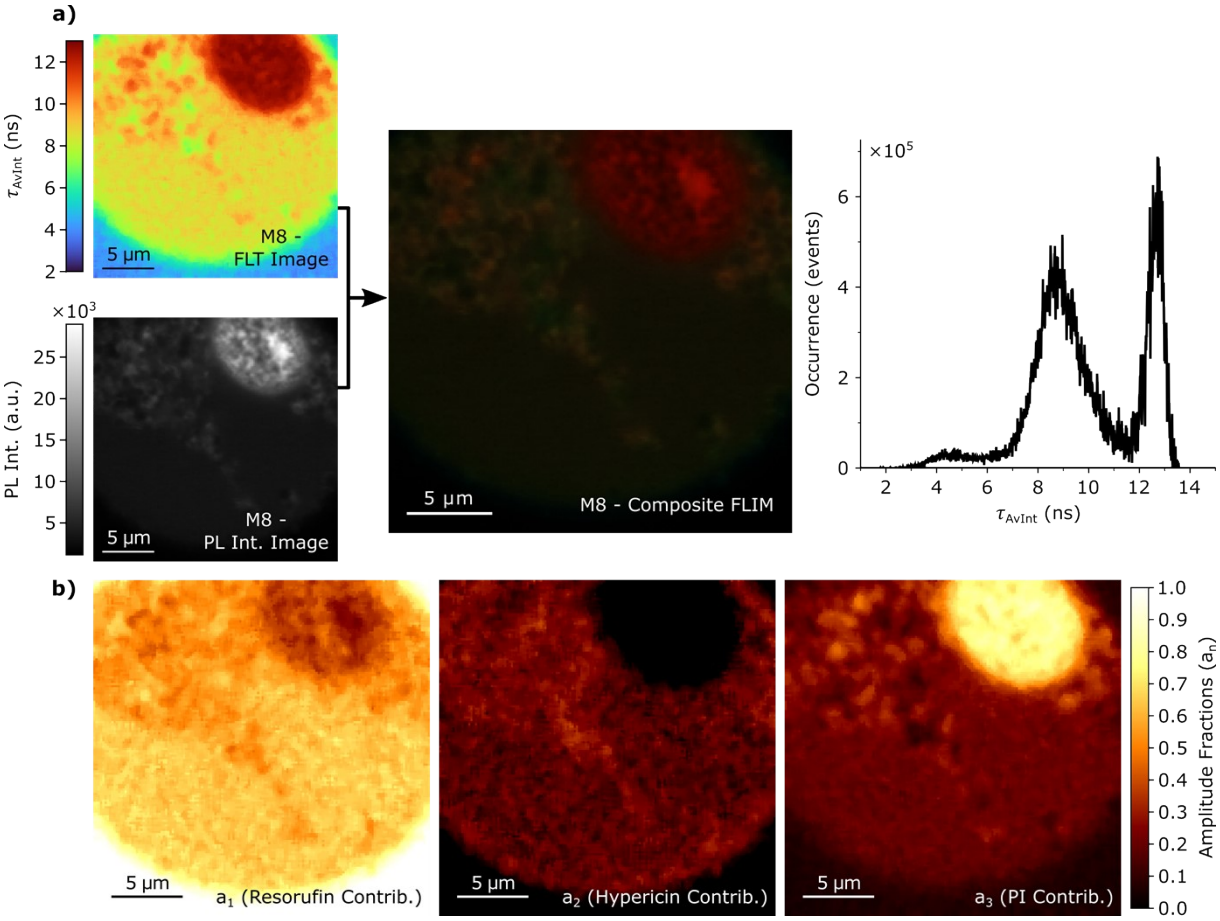

Figure S6.3: *Supplementary information for Fig. 3 (main manuscript) M8. In a) the FLT image and the PL intensity image that comprise the composite FLIM image are depicted and the occurrence plot for the image's* τ_{AvInt} *values are shown. The amplitude fraction plots in b) depict the contribution of the individual dyes to the 3-exponential fit of the overall photoluminescence decay at each pixel of the FLIM image.*

At this last stage of the series, PI dominates the fluorescence of the cell, as evident from the FLIM images and the occurrence plot on the right-hand side of Fig. S6.3a, as well as the spatially resolved spectra (see Fig. 4 of the main manuscript). The ER is completely degraded, and the cell is flooded with the surrounding medium.

Section 7 – Additional Confocal Measurement of a Cell Incubated with Hypericin, Resorufin and Propidium Iodide

In the following, an additional composite FLIM image sequences of hypericin induced PDT on a glioma cell incubated with all three fluorescent markers is depicted. The PDT progresses similarly to what is reported for another cell in another sample under similar conditions in the main manuscript (Fig. 3). This similarity in the progression of the PDT was reproducible for all investigated cells.

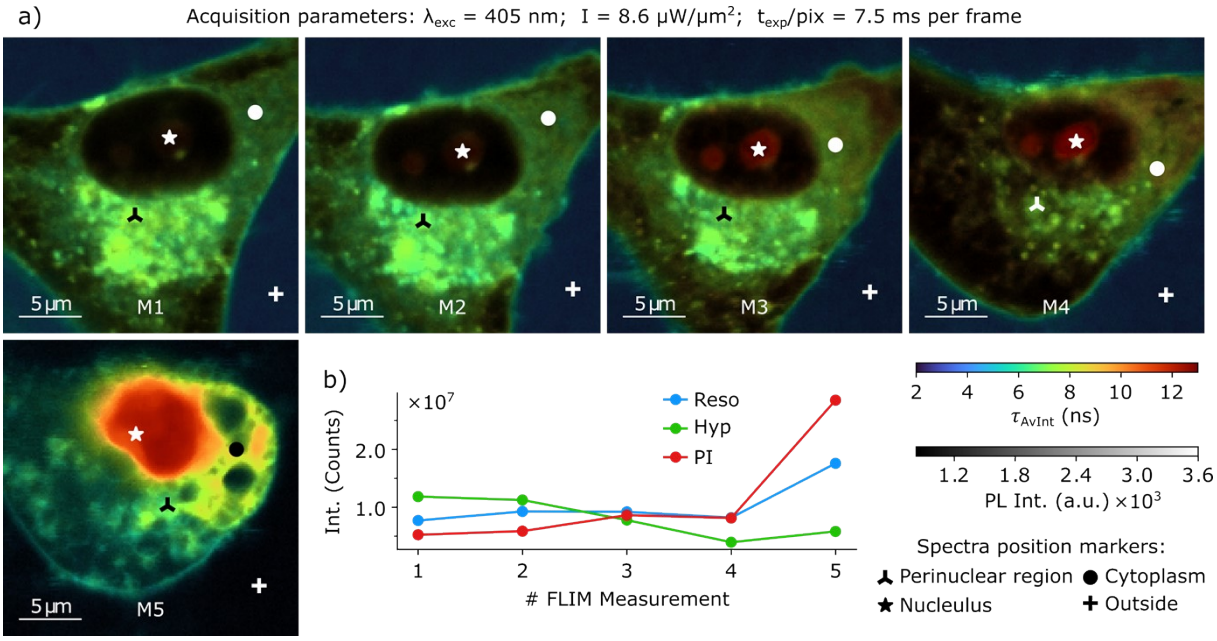

Figure S7.1: *a) Composite FLIM image series of a single glioma cell after hypericin incubation, PI supplementation and resorufin conversion. b) The evolution of the PL intensity emitted by the individual dyes in the FLIM image series. The acquisition parameters of the imaging series are displayed above. The spectra corresponding to the position markers are displayed in Fig. S7.2.*

The initially triangular cell in Fig. S7.1a M1 shows the highest hypericin accumulation in the ER with τ_{AvInt} values of approx. 7 ns. The cytoplasm reveals a homogeneous average lifetime of approx. 6 ns, which corresponds to an average FLT of hypericin, resorufin and a miniscule amount of PI, which can already be found in the nucleoli ($\tau_{AvInt} \approx$ 12 ns). Resorufin dominates the fluorescence of the surrounding medium ($\tau_{AvInt} \approx$ 3 ns). As the PDT progresses during the series, we observe degradation of the ER and a continuously increasing uptake of PI. The PDT induces morphological changes, such as cell body shrinkage, rounding and membrane blebbing. The small surface blebs merge and form a large protuberance of the cellular membrane in M4. In M5, PI is highly enriched inside the whole nucleus and the cytoplasm as evident from the spectra in Fig. S7.2. We also observe easing of the membrane stability and signs of beginning flooding with the surrounding medium.

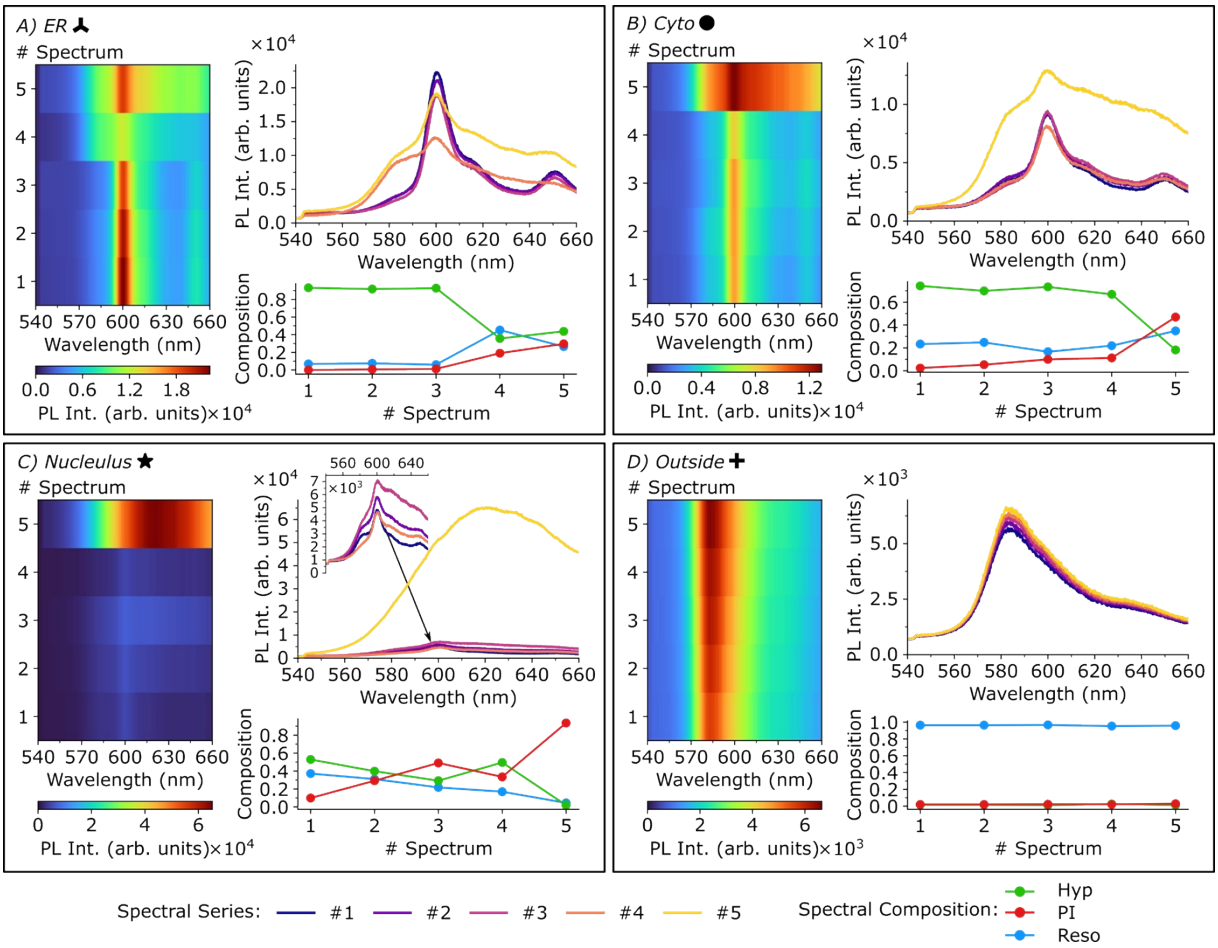

Figure S7.2: *Spatially resolved fluorescence spectra recorded on the exact locations of the corresponding markers in Figure S7.1. All spectra were acquired at the wavelength and laser power used for the FLIM image acquisition (405 nm, I = 8.6 µw/µm²) with an integration time of one second.*

Section 8 – Spectral Unmixing

Spectral unmixing is a method to decompose a spectrum consisting of multiple components into a set of individual components and their respective contribution to the total spectrum. For this purpose, it is assumed, that the total spectrum I_{tot} is a linear combination of individual spectra:

$$I_{tot} = a_{Hyp} I_{Hyp} + a_{Res} I_{Res} + a_{PI} I_{PI},$$

where $I_{Hyp}/I_{Res}/I_{PI}$ are experimentally measured spectra of Hypericin, Resorufin and PI, respectively. This linear equation was solved with MatLab to determine the contributions of the individual components $a_{Hyp}/a_{Res}/a_{PI}$.

Section 9 – Transient Absorption Measurements

Not limited by the emission of photons, femtosecond transient absorption spectroscopy (TAS) was used to verify the non-emissive triplet transition and subsequent oxygen quenching in hypericin in DMSO (deaerated and ambient conditions) and in biological medium.

An Astrella-F ultrafast Ti:sapphire amplifier from Coherent was used to generate 90 fs excitation pulses at a central wavelength of 800 nm with a repetition rate of 1 kHz. The excitation wavelength was altered to monochromatic 480 nm (fourth harmonic idler) and 0.3 µJ per pulse by using an Apollo-T optical parametric amplifier from Ultrafast Systems. The nanosecond transient absorption spectrometer EOS Fire from Ultrafast Systems was used to generate a broadband white-light probe continuum from 380 to

820 nm with a photonic crystal fiber and to control the pump-probe delay electronically up to 450 µs. Pump and probe beam were focused on a quartz glass 2 mm microcuvette from Hellma Analytics equipped with a magnetic stir bar. A part of the probe beam was split off in front of the sample and directed to the detector without going through the sample. This reference pulse was used to account for pulse-to-pulse fluctuations. An optical noise-corrected difference absorption spectrum (ΔA) as a function of delay time (T_D) and wavelength (λ) was calculated by subtracting the noise-corrected absorption spectrum of the excited sample ($A^{exc.}$) from the corrected ground state absorption spectrum of the unexcited sample (A^{ground}) as follows:

$$\Delta A(\lambda, T_D) = A^{exc.}(\lambda, T_D) - A^{ground}(\lambda) \ .$$

All samples were diluted to 0.025 for DMSO and 0.09 absorbance in medium at 480 nm respectively. To avoid non-linear processes and dimerization, both, energy, and concentration were chosen to be more than one order of magnitude smaller compared to experiments from literature where slightly saturated one-photon processes were observed [9]. Steady-state absorption and photoluminescence spectra were acquired before and after each TAS experiment to ensure that no significant sample degradation occurs during the irradiation. The background scattered light substraction and kinetic fitting was performed with the software Surface Xplorer from Ultrafast Systems, while Python 3.9 was used for visualization.

Kinetic traces were fitted with a parallel kinetic model at selected wavelengths with a sum of exponentials convoluted with the IRF according to the following equation

$$\Delta A(T_D, \lambda = const.) = e^{-\left(\frac{T_D - t_0}{\frac{IRF}{2ln2}}\right)^2} * \sum_i A_i e^{-\frac{T_D - t_0}{\tau_i}} \ ,$$

where ΔA is the differential absorption at a given wavelength λ, T_D the pump-probe delay time, t_0 time zero, IRF the instrument response function, A_i the amplitude and τ_i the decay time of component i.

The absolute photoluminescence quantum yield was measured with a fluorescence spectrometer FL8500 from PerkinElmer equipped with an integration sphere. The samples were diluted below 0.05 absorbance at 480 nm in a standard 10 mm quartz glass cuvette at room temperature. The quantum yield was calculated according to

$$PLQY = \frac{E_d - E_{sol}}{S_{sol} - S_d} \ ,$$

where PLQY is the photoluminescence quantum yield, E_d and E_{sol} are the integrated emission signals of the sample and the blank solvent respectively, S_d and S_{sol} are the integrated scattering signals of the sample and the solvent.

Figure S9.1 shows the results of the TAS study of hypericin in oxygen-free DMSO (Fig. S9.1a+b), in DMSO under ambient conditions (Fig. S9.1c) and in medium under ambient conditions (Fig. S9.1d). For comparison, the steady-state absorption (red) and photoluminescence (blue) of the investigated sample is displayed above the plots. The magnitude and sign of the differential absorption is color coded. While grey means no change in absorption of the excited sample compared to the sample in the ground state, red means a gain in absorbance or excited-state absorption and blue means a loss in absorption or bleach. The spectral regions between 470 and 490 nm are left blank due to strong scattering of the excitation pulse at 480 nm. Fig. S9.1b represents ΔA spectra at selected delay times of Fig. S9.1a allowing for a better visualization of the spectral shape and evolution of the transient signals. The kinetic traces recorded at 520 nm, indicated by solid lines in the surface plots for all three samples, are shown in Fig. S9.1e. This wavelength is suited for monitoring the triplet transition, since the interfering contributions of scattered light and emission are minimal here.[10] Up to four exponential components were needed to satisfactorily fit the data. The fitting results are summarized in Table S9.

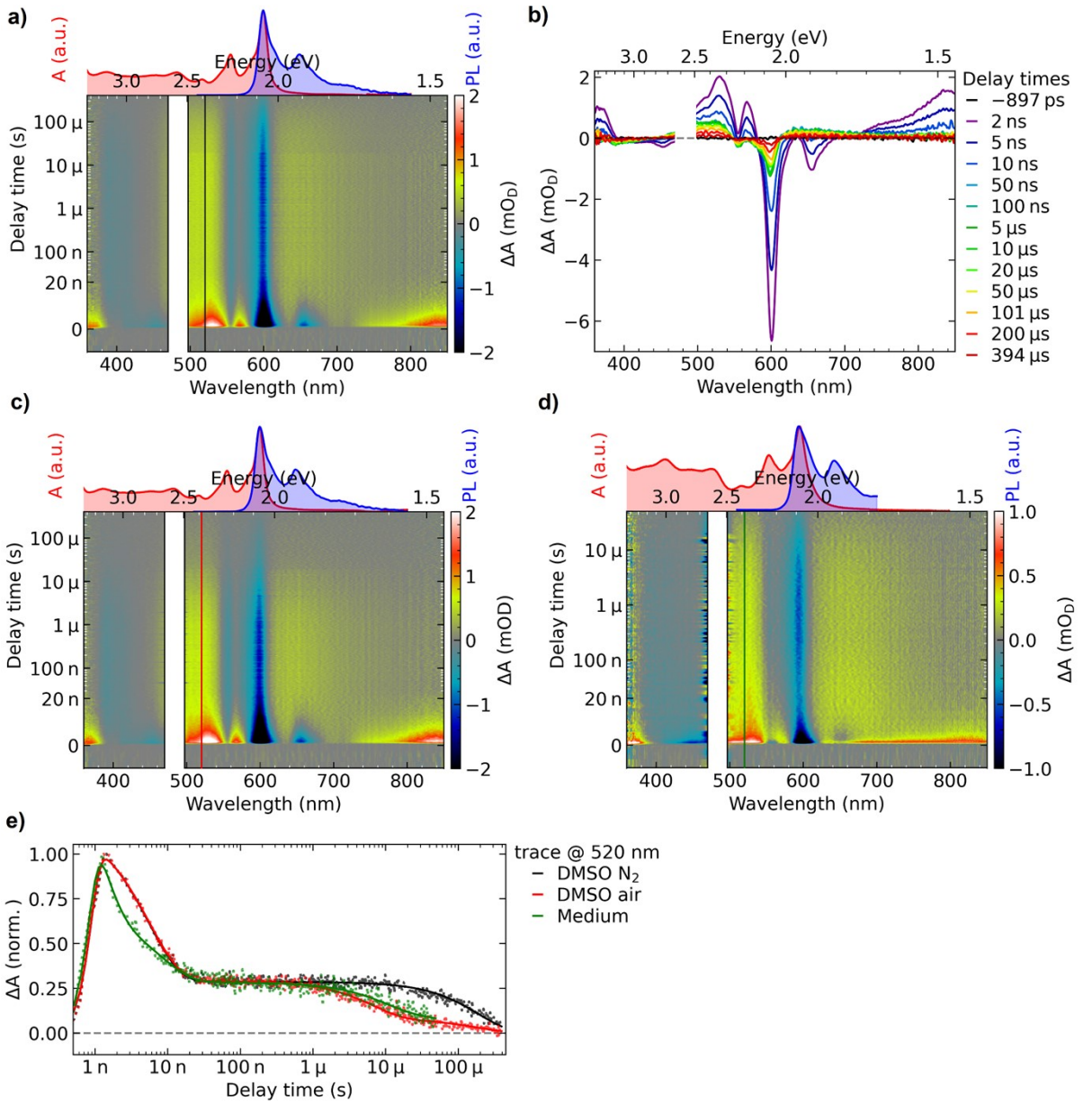

Figure S9.1: *Transient absorption spectra of Hypericin in DMSO under inert conditions (a+b), in DMSO under ambient conditions (c) and in medium under ambient conditions (d). All samples were excited at 480 nm with an energy of 0.3 µJ/pulse. In the 2D plots, the wavelength is plotted against the delay time while the differential absorbance is color coded. The first 20 ns are shown in a linear scale followed by a logarithmic time scale. Steady-state absorbance (red) and photoluminescence (blue) of the samples are shown above the plots. In (b), spectral slices of (a) are shown at selected delay times. (e) shows kinetic traces at 520 nm of Hypericin under the different conditions (dotted) as well as the related fit functions (solid line).*

Table S9: *Summary of the decay fit components (lifetime τ and relative amplitude A) at 520 nm of Hypericin under different conditions using a sum of two to four exponentials convoluted with the IRF. σ_{norm} is the normalized standard deviation.*

Fit Component	**DMSO N_2**	**DMSO air**	**Medium**
IRF	0.68 ns	0.6 ns	0.59 ns
τ_1 A_1	-	-	0.8 ns 50 %
τ_2 A_2	5.5 ns 73 %	5.6 ns 72 %	8 ns 28 %
τ_3 A_3	-	6.6 µs 20 %	10 µs 14 %
τ_4 A_4	191 µs 27 %	190 µs (fixed) 8 %	190 µs (fixed) 8 %
σ_{norm}	0.02	0.02	0.03

By comparison with the steady-state absorption and photoluminescence spectra, we interpret the negative ΔA features around 600 nm and 655 nm in all three samples as a combined ground state bleach and stimulated emission. All samples remain in an excited state, indicated by reaching a plateau at non-zero ΔA values after 20 ns (Fig. S9.1e). In DMSO, the spectral shapes and decay dynamics within the first 20 ns show no differences with or without the presence of oxygen (a+c). In medium, the TA spectrum is qualitatively similar within this time window, but the decay is faster. This is illustrated by the lifetimes τ_1 and τ_2 in Table S9, obtained from fitting the data in the first 20 ns in Figure S9.1 e). While hypericin in DMSO decays monoexponentially with τ_2 = 5.5 ns (deaerated) or 5.6 ns (ambient), the decay in medium is biexponential with τ_1 = 0.8 ns and τ_2 = 8 ns. Calculating the intensity weighted average lifetime of this biexponential radiant decay according to S1.1 yields:

$$\tau_{AvInt} = \frac{\sum_{n=1}^{m} a_n \tau_n^{\,2}}{\sum_{n=1}^{m} a_n \tau_n} = \frac{\frac{50}{78} * 0.8^2 + \frac{28}{78} * 8^2}{\frac{50}{78} * 0.8 + \frac{28}{78} * 8} ns = 6.9\ ns$$

These values are in good agreement with the average fluorescence lifetime measurements of 5.4 ns in DMSO (Fig. S2.4) and 6.8 ns in medium (Fig S2.2). We note that there are no other additional kinetics in DMSO under inert conditions in this time regime.

For longer delay times of several microseconds, a second decay is evident, the dynamics of which are dominated by the presence/absence of oxygen. In deaerated DMSO, this decay is monoexponential with τ_4 = 191 µs. Under ambient conditions, the decay is biexponential with τ_3 = 6.6 µs (in DMSO) or 10 µs (in medium) and τ_4 = 190 µs. All samples reach the ground state after this second decay period. We do not observe the formation of the radical anion, which would be expected to occur at 740 nm with an extensive lifetime of several hundred microseconds.[10]

We interpret the fast decay component (τ_2) with the decay of a singlet state of hypericin. This decay is mostly radiative, evidenced by the good agreement of the lifetimes with the time-resolved PL measurements presented here. Note that the expected fluorescence quantum yield of hypericin under these conditions is 45 to 50 %.[9, 11] The biexponential decay of the singlet in medium suggests fast

additional quenching (τ_1), which is also reflected in the poor fluorescence quantum yield below 5 %. This might be due to interaction with the medium (buffer, ions etc.) or the formation of aggregates. The presence of oxygen does not affect the singlet fluorescence.

We suggest that the long decay component (τ_4) is caused by relaxation from a triplet state to the ground state, which is expected to form with a quantum yield of 50 to 70 %.[12] Our data indicates that both, fluorescence and intersystem crossing, occur with roughly the same rate constants. In the presence of oxygen, strong quenching of the triplet state occurs, presumably due to the formation of ROS with τ_3.

Section 10 – Further Widefield Fluorescence Imaging Series

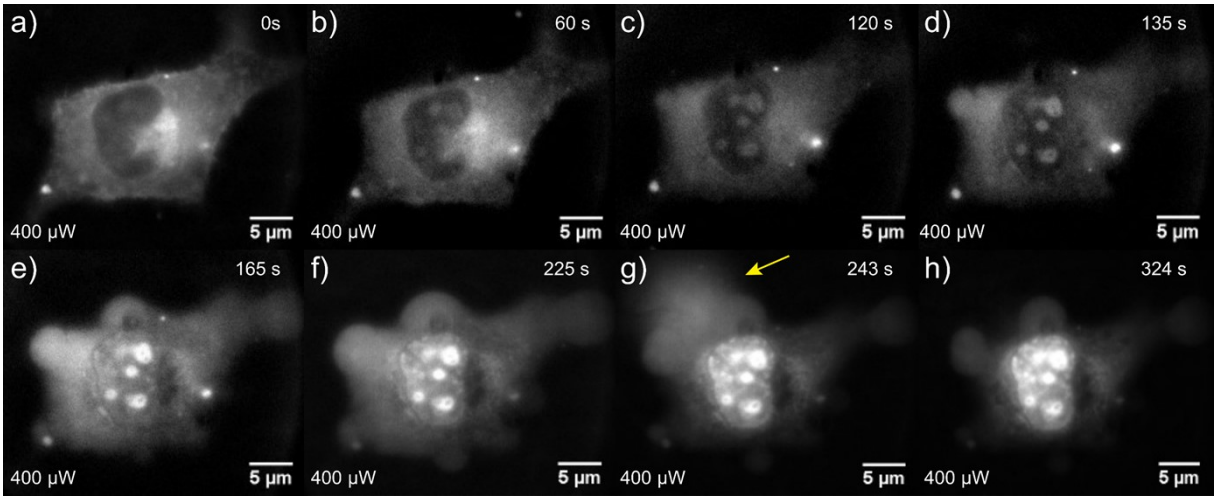

Figure S10.1: *Series of widefield fluorescence images showing the effect of hypericin induced PDT on a single glioma cell incubated with hypericin and PI.*

R**eferences:**

1. J. R. Lakowicz, *Principles of Fluorescence Spectroscopy*, Springer Science+Business Media, New York, 3 edn., 2007.
2. D. O'Connor, *Time-correlated single photon counting*, Academic press, 2012.
3. W. Becker, *Advanced time-correlated single photon counting techniques*, Springer Science & Business Media, 2005.
4. M. Kasha, *Discuss. Faraday Soc.*, 1950, **9**, 14-19.
5. A. Sillen and Y. Engelborghs, *Photochemistry and Photobiology*, 1998, **67**, 475-486.
6. A. E. McKinnon, A. G. Szabo and D. R. Miller, *The Journal of Physical Chemistry*, 1977, **81**, 1564-1570.
7. J. T. Giurleo and D. S. Talaga, *The Journal of Chemical Physics*, 2008, **128**, 114114.
8. A. Grinvald and I. Z. Steinberg, *Analytical Biochemistry*, 1974, **59**, 583-598.
9. A. Michaeli, A. Regev, Y. Mazur, J. Feitelson and H. Levanon, *The Journal of Physical Chemistry*, 1993, **97**, 9154-9160.
10. P. López-Chicón, M. P. Paz-Cristobal, A. Rezusta, C. Aspiroz, M. Royo-Cañas, E. Andres-Ciriano, Y. Gilaberte, M. Agut and S. Nonell, *Photochemical & Photobiological Sciences*, 2012, **11**, 1099-1107.
11. B. Ehrenberg, J. L. Anderson and C. S. Foote, *Photochemistry and Photobiology*, 1998, **68**, 135-140.
12. M. Roslaniec, H. Weitman, D. Freeman, Y. Mazur and B. Ehrenberg, *J. Photochem. Photobiol. B: Biol.*, 2000, **57**, 149-158.